Interaction of twisted light with a trapped atom: Interplay between electronic and motional degrees of freedom

A. A. Peshkov,[1,2,*] Y. M. Bidasyuk,[1] R. Lange,[1] N. Huntemann,[1] E. Peik,[1] and A. Surzhykov[1,2,3]

[1]*Physikalisch-Technische Bundesanstalt, D-38116 Braunschweig, Germany*

[2]*Institut für Mathematische Physik, Technische Universität Braunschweig, D-38106 Braunschweig, Germany*

[3]*Laboratory for Emerging Nanometrology Braunschweig, D-38106 Braunschweig, Germany*

(Received 22 July 2022; accepted 25 January 2023; published 13 February 2023)

We present a theoretical study of nondipole excitation of a single trapped atom by twisted light. Special emphasis is placed on effects that arise from the interplay between internal (electronic) and vibrational (center-of-mass) degrees of freedom of an atom. In order to provide a fully quantum mechanical understanding of the excitation, we used the density-matrix approach based on the Liouville–von Neumann equation. The developed theory has been applied to the particular case of the $4s\ ^2S_{1/2} \rightarrow 3d\ ^2D_{5/2}$ electric quadrupole ($E2$) transition in a $^{40}Ca^+$ ion induced by Laguerre-Gaussian modes. It was found that the Rabi oscillations can show unconventional anharmonic behavior that is attributed to the strong coupling between vibrational levels of the trap. This effect is accompanied by the transfer of angular momentum to the center-of-mass motion and becomes most pronounced when the Rabi frequency is comparable to the trapping frequency.

DOI: 10.1103/PhysRevA.107.023106

I. INTRODUCTION

Techniques for the manipulation of trapped atoms or ions are of great interest due to their applications in atomic clocks [1], searches for new physics [2,3], quantum computing [4], and quantum sensing [5,6]. At the heart of these applications is the use of selective resonance excitation of an atom by light. In the time domain, the excitation process manifests itself as Rabi oscillations of atomic populations [7]. This phenomenon is best understood in the case of conventional "plane-wave" radiation for which the variations in the beam intensity profile are negligible compared to the size of an atomic absorber [8,9]. Significantly less is known, however, about the mechanism of Rabi oscillations for an atom exposed to high-order laser modes that have a strongly inhomogeneous internal structure [10].

Radiation having a helical phase front and a ringlike intensity profile with a central dark spot gives a good example of inhomogeneous high-order modes [11–13]. This so-called twisted light is particularly interesting because of its ability to carry a nonzero projection of the orbital angular momentum (OAM) upon the propagation direction [14–16]. Twisted light has found applications in areas as diverse as waveguides for cold atoms [17–19], optical traps [20–22], quantum memory [23–25], super-resolution optical sensing [26], and cryptographic schemes [27–29].

The first experiment on excitation of single trapped ions by twisted light was reported in 2016 [30]. This research has attracted considerable interest in the field of precision spectroscopy, since the atomic excitation in the low-intensity center of a twisted beam can suppress the undesirable light shift and efficiently induce dipole-forbidden transitions [30,31]. Analysis of Rabi oscillations for such "excitation in the darkness" experiments is, however, complicated due to the fact that an atom is locally exposed to different electric fields as it moves within the beam cross section.

Various theoretical approaches have been developed in the past to analyze the influence of a position of an atom on its interaction with twisted radiation. In the semiclassical approach the atom's internal degrees of freedom are described quantum mechanically, while its center of mass is assumed to have a well-defined impact parameter with respect to the beam center [32–37]. This semiclassical method was successfully applied to investigate how the polarization and OAM of twisted light can affect the photoexcitation of different atoms and ions [38–40]. Moreover, extensions of the theory to experimentally relevant scenarios of uniform [41,42] and Gaussian [43,44] spatial distributions of an atom have been proposed.

In contrast to the semiclassical approach, the rigorous treatment of the twisted light-trapped atom interaction requires quantum mechanical description of both internal and center-of-mass degrees of freedom [45–53]; the interested reader is referred to a recent review [54]. Within such a theory the center-of-mass motion is described with the help of oscillator eigensolutions for an external trapping potential. In the past this approach has mainly been used to study the excitation of electric dipole transitions [55,56], which are important, for example, for manipulating atomic Bose-Einstein condensates [57,58]. Much less attention has been paid, however, to the dipole-forbidden transitions that are of special interest for high-precision atomic spectroscopy and development of a new generation of atomic clocks. In this contribution, therefore, we present a rigorous quantum mechanical approach to investigate the effects of center-of-mass motion on the nondipole coupling of atoms and twisted light. We explore

*anton.peshkov.ext@ptb.de

a scenario in which a single atom is placed in a harmonic trap and is irradiated by a Laguerre-Gaussian (LG) mode. A fully quantum mechanical description of the atomic vibrational (center-of-mass) and internal (electronic) states is based on the Hamiltonian of the combined atom-*plus*-trap system, which is briefly reviewed in Sec. II A. The perturbation of the system induced by LG modes is then discussed in Sec. II B. In order to describe the time evolution of the internal and vibrational states of an atom, we employ in Sec. II C the density-matrix approach based on the Liouville-von Neumann equation. The solution of this equation requires knowledge of the matrix elements for transitions between electronic and vibrational levels whose evaluation is discussed in Sec. II D with a focus on nondipole coupling. While the developed approach can be applied to any atomic system, we consider here a particular case of the $4s\ ^2S_{1/2} \rightarrow 3d\ ^2D_{5/2}$ electric quadrupole ($E2$) transition in the $^{40}Ca^+$ ion. Its excitation, especially when accompanied by a change in the transverse ion motion, is currently of particular experimental interest [59]. For this $E2$ transition, theoretical predictions for the Rabi oscillations are presented and discussed in Sec. III. Finally, a summary of our results and an outlook to future work are given in Sec. IV.

II. THEORY

A. Atom in a trap

Before delving into the details of the photoexcitation process, it is instructive to discuss the system of interest in the absence of light fields. We consider a single alkalilike atom or ion placed in a trapping potential $\hat{\mathcal{V}}_{\rm trap}$. The Hamiltonian of such a system can in general be written as

$$\hat{H}_0 = \hat{H}_{\rm cm} + \hat{H}_{\rm atom}, \tag{1}$$

where $\hat{H}_{\rm cm}$ characterizes the motion of an atom, and $\hat{H}_{\rm atom}$ describes its internal electronic structure. The operator $\hat{H}_{\rm cm}$ reads

$$\hat{H}_{\rm cm} = -\frac{\hbar^2}{2\mathfrak{m}_{\rm a}}\nabla_R^2 + \hat{\mathcal{V}}_{\rm trap}(\boldsymbol{R}), \tag{2}$$

with $\boldsymbol{R}$ and $\mathfrak{m}_{\rm a}$ being, respectively, the atomic center-of-mass coordinate and its total mass [60]. In order to obtain the explicit form of $\hat{H}_{\rm cm}$, it is necessary to agree on the trap parameters. We assume a trapping potential of the form

$$\hat{\mathcal{V}}_{\rm trap}(\boldsymbol{R}) = \tfrac{1}{2}\mathfrak{m}_{\rm a}\left(\omega_{\rm r}^2 R_\perp^2 + \omega_{\rm z}^2 Z^2\right), \tag{3}$$

where $\boldsymbol{R} = (R_\perp \cos\Phi,\ R_\perp \sin\Phi,\ Z)$. Equation (3) implies that an atom undergoes harmonic motion in the xy plane with an oscillation frequency $\omega_{\rm r}$. Moreover, we suppose that $\omega_{\rm z} \gg \omega_{\rm r}$, so the atomic motion in the z direction is confined to a negligibly small distance about $Z = 0$ (see Fig. 1). For such a disk-shaped potential, Eq. (2) may be rewritten as

$$\hat{H}_{\rm cm} = -\frac{\hbar^2}{2\mathfrak{m}_{\rm a}}\nabla_{R_\perp}^2 + \frac{1}{2}\mathfrak{m}_{\rm a}\omega_{\rm r}^2 R_\perp^2. \tag{4}$$

This harmonic approximation is commonly used for atoms moving near the center of the trap [61].

The operator (4) is nothing else but the well-known Hamiltonian of a two-dimensional oscillator [62]. Its eigenfunctions can be expressed in terms of associated Laguerre polynomials

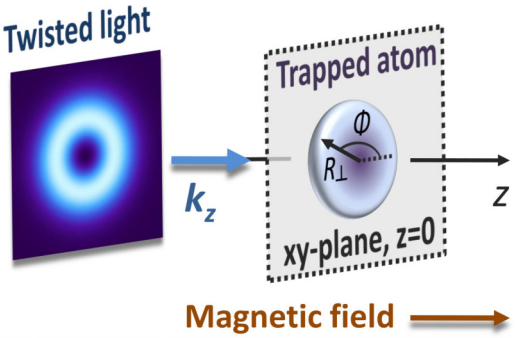

FIG. 1. Geometry for the excitation of a single trapped atom by twisted light. The quantization axis is chosen to be along the applied magnetic field and the trap's z axis. Twisted light also propagates in the z direction, and the beam axis coincides with the trap's center. The atom is moving in the xy plane, while its motion in the z direction is frozen at $Z = 0$. The polar coordinates $R_\perp$ and Φ define the atomic center-of-mass position. The drawing is not to scale; the beam diameter is much larger than the atomic target size.

as

$$U_{nl}(\boldsymbol{R}_\perp) = u_{nl}(R_\perp)\, e^{il\Phi} = \sqrt{\frac{n!}{\pi b^2 (n+|l|)!}}\, \frac{R_\perp^{|l|}}{b^{|l|}}\, e^{-\frac{R_\perp^2}{2b^2}}\, L_n^{|l|}(R_\perp^2/b^2)\, e^{il\Phi}, \tag{5}$$

where we have introduced the harmonic oscillator length $b = \sqrt{\hbar/(\mathfrak{m}_{\rm a}\omega_{\rm r})}$. The corresponding energy eigenvalues

$$E_{nl} = \hbar\omega_{\rm r}(2n + |l| + 1) \tag{6}$$

are labeled by the vibrational quantum numbers n and l. Here the positive integer n is related to the number of nodes of the function (5), and the integer l denotes the OAM projection of the atomic motion on the trap's z axis.

In addition to the center-of-mass Hamiltonian (4), we also need to specify its internal structure counterpart $\hat{H}_{\rm atom}$. The explicit form of $\hat{H}_{\rm atom}$ depends, of course, on a particular atom. For simplicity, we consider here an alkalilike atom with one electron outside of a closed shell. To describe such a system, we assume that the outer electron moves in a frozen potential $\hat{W}$ produced by the nucleus and the remaining electrons. Moreover, $\hat{W}$ incorporates the spin-orbit interaction to account for the fine structure; transitions between fine-structure levels are often of experimental interest. Within this single-active-electron approximation the atomic Hamiltonian is given by

$$\hat{H}_{\rm atom} = -\frac{\hbar^2}{2\mu}\nabla_r^2 + \hat{W}(\boldsymbol{r}), \tag{7}$$

where $\mu = \mathfrak{m}_e\mathfrak{m}_{\rm n}/(\mathfrak{m}_e + \mathfrak{m}_{\rm n})$ stands for the reduced mass, and $\boldsymbol{r}$ is the relative coordinate of the outer electron of mass $\mathfrak{m}_e$ with respect to the nucleus, whose mass together with the remaining electrons is $\mathfrak{m}_{\rm n}$ [60].

Not much needs to be said about the eigenfunctions $\psi_{\alpha JM}(\boldsymbol{r})$ and eigenenergies $E_{\alpha JM}$ of $\hat{H}_{\rm atom}$. They satisfy the equation $\hat{H}_{\rm atom}\psi_{\alpha JM}(\boldsymbol{r}) = E_{\alpha JM}\psi_{\alpha JM}(\boldsymbol{r})$ and are characterized by the total electronic angular momentum J, its projection M, and all additional quantum numbers α. In our study, the

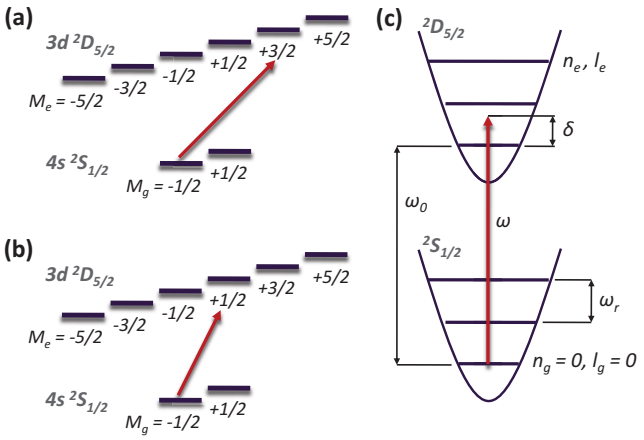

FIG. 2. Excitation of the $4s\ ^2S_{1/2} \to 3d\ ^2D_{5/2}$ electric quadrupole transition in $^{40}Ca^+$. Shown are transitions between individual magnetic sublevels (a) $M_g = -1/2 \to M_e = +3/2$ and (b) $M_g = -1/2 \to M_e = +1/2$, which are separated by the Zeeman effect. (c) Energy levels of a two-level atom in a two-dimensional harmonic trap with oscillation frequency ω_r. The vibrational levels in the ground and excited electronic states are labeled by the quantum numbers n_g, l_g and n_e, l_e, respectively. The atom is assumed to be initially in the lowest vibrational and electronic state, while the light frequency ω is slightly detuned from the transition frequency ω_0 for a free atom by $\delta = \omega - \omega_0$.

$(2J+1)$ degeneracy with respect to M is removed by applying a magnetic field parallel to the trap's z axis, which also provides the quantization axis of the overall system. The resulting Zeeman splitting will allow us to reduce the system to only two magnetic sublevels that are coupled by a near-resonant radiation field, thereby greatly simplifying the calculations (see Fig. 2).

Since the Hamiltonian of a trapped atom (1) is made up of a term (4) involving only the center-of-mass coordinate $\boldsymbol{R}_\perp$ and a term (7) depending only on the relative coordinate $\boldsymbol{r}$, its eigenfunction is factorizable into a product:

$$\begin{aligned}\Psi_{nl,\alpha JM}(\boldsymbol{R}_\perp, \boldsymbol{r}) &= \langle \boldsymbol{R}_\perp | nl \rangle \, \langle \boldsymbol{r} | \alpha JM \rangle \\ &\equiv U_{nl}(\boldsymbol{R}_\perp)\, \psi_{\alpha JM}(\boldsymbol{r}). \end{aligned} \tag{8}$$

This factorization can be seen as a reflection of the fact that the trap potential changes very little on the atomic scale. The wave function (8) is a solution of the equation

$$\hat{H}_0\, \Psi_{nl,\alpha JM}(\boldsymbol{R}_\perp, \boldsymbol{r}) = E_{nl,\alpha JM}\, \Psi_{nl,\alpha JM}(\boldsymbol{R}_\perp, \boldsymbol{r}), \tag{9}$$

with $E_{nl,\alpha JM} = E_{nl} + E_{\alpha JM}$ being the total energy of the system.

B. Twisted light

Let us now turn to the interaction between a trapped atom and twisted radiation. Here we utilize a circularly polarized Laguerre-Gaussian mode with zero radial index, LG_{0m}, which is often used in experimental studies [15,30]. This beam is also characterized by the frequency $\omega = ck$, the waist w_0, the helicity $\lambda = \pm 1$, and the OAM projection m. It is assumed that the beam propagates parallel to the quantization (z) axis. Herewith the waist plane $z = 0$ is superimposed on the plane of atomic motion and the beam center coincides with the trap center (see Fig. 1). The vector potential of the LG_{0m} beam may be written in the Coulomb gauge as

$$\boldsymbol{A}^{(\mathrm{tw})}(\boldsymbol{r}) = A_0 \int a_m(k_\perp)\, e^{i(m+\lambda)\phi_k}\, \boldsymbol{e}_{\boldsymbol{k}\lambda}\, e^{i\boldsymbol{k}\boldsymbol{r}}\, \frac{d^2\boldsymbol{k}_\perp}{2\pi}, \tag{10}$$

where A_0 is the amplitude to be determined later, and the weight function $a_m(k_\perp)$ reads

$$a_m(k_\perp) = (-i)^{|m|} \sqrt{\frac{2}{\pi\, w_0^2 |m|!}}\, \frac{w_0^{|m|+2}\, k_\perp^{|m|}}{2^{|m|/2+1}}\, e^{-\frac{k_\perp^2 w_0^2}{4}} \tag{11}$$

(see Refs. [34,35] for more details). Equations (10) and (11) imply that the Laguerre-Gaussian mode can be seen as a superposition of plane waves whose polarization vector

$$\boldsymbol{e}_{\boldsymbol{k}\lambda} = \frac{1}{\sqrt{2}} \begin{pmatrix} \cos\theta_k \cos\phi_k - i\lambda \sin\phi_k \\ \cos\theta_k \sin\phi_k + i\lambda \cos\phi_k \\ -\sin\theta_k \end{pmatrix} \tag{12}$$

and wave vector $\boldsymbol{k} = (k_\perp \cos\phi_k,\ k_\perp \sin\phi_k,\ k_z)$ are orthogonal to each other, $\boldsymbol{k} \cdot \boldsymbol{e}_{\boldsymbol{k}\lambda} = 0$ [63,64]. Such a decomposition of the electromagnetic field into plane waves is widely used in atomic and optical physics [65,66].

Nowadays the twisted beams are usually produced in the paraxial regime in which $\boldsymbol{k}$ is inclined by a small angle $\theta_k = \arctan(k_\perp/k_z)$ with respect to the z axis [10]. In this case, Eq. (12) can be approximated by

$$\boldsymbol{e}_{\boldsymbol{k}\lambda} \approx e^{-i\lambda\phi_k}\, \boldsymbol{\xi}_\lambda, \tag{13}$$

where $\boldsymbol{\xi}_\lambda \equiv \boldsymbol{e}_{\boldsymbol{k}\lambda}(\theta_k = 0,\ \phi_k = 0) = (1,\ i\lambda,\ 0)/\sqrt{2}$ is just the polarization vector of a circularly polarized plane wave propagating in the z direction [67]. By using Eq. (13) and applying a standard integral representation of the Bessel function [41]

$$\int_0^{2\pi} e^{in\phi + iz\cos\phi}\, \frac{d\phi}{2\pi} = i^n\, J_n(z) \tag{14}$$

along with the relation [68]

$$x^n\, e^{-x} = \int_0^\infty (\sqrt{xt})^n\, J_n(2\sqrt{xt})\, e^{-t}\, dt, \tag{15}$$

we evaluate the integral (10) and obtain the well-known result for the LG_{0m} mode

$$\boldsymbol{A}^{(\mathrm{tw})}(r_\perp, \phi) \approx \boldsymbol{\xi}_\lambda\, A_0 \sqrt{\frac{2}{\pi\, w_0^2 |m|!}} \left(\frac{r_\perp \sqrt{2}}{w_0}\right)^{|m|} e^{-r_\perp^2/w_0^2}\, e^{im\phi} \tag{16}$$

at the waist plane $z = 0$ where the atom is located [12]. By means of Eq. (16) one can determine the intensity I of the light beam and its total power P [7]. The intensity I is proportional to the modulus squared of the vector potential and is independent of the azimuthal angle ϕ:

$$I(r_\perp) = \tfrac{1}{2} c\epsilon_0 \omega^2\, |\boldsymbol{A}^{(\mathrm{tw})}(r_\perp, \phi)|^2. \tag{17}$$

The total power

$$P = \int I(r_\perp)\, d^2\boldsymbol{r}_\perp \tag{18}$$

is given by an integral of the intensity I over the beam cross section [69]. From these identities, we define the amplitude of

the LG_{0m} mode as

$$A_0 = \sqrt{\frac{2P}{c\epsilon_0\omega^2}}. \tag{19}$$

This expression, together with Eq. (11), provides a link between the dynamics of the excitation process and the experimentally controlled light power and waist.

Having discussed the vector potential of the twisted light, we can now evaluate its effect on a trapped atom. To do this we recall that the nuclear mass $\mathfrak{m}_\mathrm{n}$ is much larger than the electron mass $\mathfrak{m}_e$. Hence the interaction can be restricted to that between radiation and electrons [60]. Within the model (7) the interaction Hamiltonian for the optically active electron takes the following form:

$$\hat{H}_\mathrm{I}(t) = \tfrac{1}{2}[\hat{V}e^{-i\omega t} + \hat{V}^\dagger e^{i\omega t}], \tag{20}$$

where $\hat{V}$ is a time-independent operator,

$$\hat{V} = -\frac{i\hbar e}{\mathfrak{m}_e}\boldsymbol{A}^{(\mathrm{tw})}(\boldsymbol{r}_e)\cdot\boldsymbol{\nabla}_{r_e}, \tag{21}$$

with $\boldsymbol{r}_e$ being the electron coordinate with respect to the trap's center. For highly inhomogeneous twisted-light fields, the dependence of the vector potential on $\boldsymbol{r}_e$ implies that the perturbation (21) is very sensitive to the atom position within the beam. Indeed, changing variables from $\boldsymbol{r}_e$ to previously defined $\boldsymbol{r}$ and $\boldsymbol{R}_\perp$ one finds

$$\begin{aligned}\hat{V} &= -\frac{i\hbar e}{\mathfrak{m}_e}\boldsymbol{A}^{(\mathrm{tw})}\left(\frac{\mathfrak{m}_\mathrm{n}}{\mathfrak{m}_\mathrm{a}}\boldsymbol{r}+\boldsymbol{R}_\perp\right)\cdot\left(\boldsymbol{\nabla}_r+\frac{\mathfrak{m}_e}{\mathfrak{m}_\mathrm{a}}\boldsymbol{\nabla}_{R_\perp}\right)\\ &\approx -\frac{i\hbar e}{\mathfrak{m}_e}\boldsymbol{A}^{(\mathrm{tw})}(\boldsymbol{r}+\boldsymbol{R}_\perp)\cdot\boldsymbol{\nabla}_r,\end{aligned} \tag{22}$$

where we have used $\mathfrak{m}_\mathrm{n}\approx\mathfrak{m}_\mathrm{a}$ and $\mathfrak{m}_e \ll \mathfrak{m}_\mathrm{a}$. Importantly, the interaction Hamiltonian (22) cannot be expressed as a sum of separate functions of $\boldsymbol{r}$ and $\boldsymbol{R}_\perp$. This means that the atom's internal dynamics is coupled to its center-of-mass motion by the light field [61].

C. Density-matrix formalism

The atomic photoexcitation is most conveniently described within the framework of the density matrix theory [70]. In this approach, the atomic system is represented by the density operator $\hat{\rho}(t)$. Its time evolution is given by the Liouville–von Neumann equation:

$$\frac{d}{dt}\hat{\rho}(t) = -\frac{i}{\hbar}[\hat{H}(t),\ \hat{\rho}(t)], \tag{23}$$

where the total Hamiltonian of the system "trapped atom *plus* light" is just the sum of the unperturbed Hamiltonian (1) and the interaction Hamiltonian (20):

$$\hat{H}(t) = \hat{H}_0 + \hat{H}_\mathrm{I}(t). \tag{24}$$

Since we focus on timescales shorter than the radiative lifetime of excited upper levels, spontaneous emission has been omitted in Eq. (23). To express the operator $\hat{\rho}(t)$ in matrix form, we choose a set of basis states $|nl, \alpha JM\rangle$ [see Eq. (8)]. The number of internal atomic states is limited to two, $|\alpha_g J_g M_g\rangle$ and $|\alpha_e J_e M_e\rangle$, between which the transition is occurring. In contrast, the number of vibrational states $|n_g l_g\rangle$ and $|n_e l_e\rangle$ associated with electronic ones is unrestricted. Within this approximation, we construct the matrix of the operator $\hat{\rho}(t)$ usually referred to as the density matrix. For the sake of shortness we use the following notation for the elements of the density matrix:

$$\rho_{gg'}(t) = \langle n_g l_g, \alpha_g J_g M_g|\hat{\rho}(t)|n'_g l'_g, \alpha_g J_g M_g\rangle, \tag{25a}$$

$$\rho_{ee'}(t) = \langle n_e l_e, \alpha_e J_e M_e|\hat{\rho}(t)|n'_e l'_e, \alpha_e J_e M_e\rangle, \tag{25b}$$

$$\rho_{ge'}(t) = \langle n_g l_g, \alpha_g J_g M_g|\hat{\rho}(t)|n'_e l'_e, \alpha_e J_e M_e\rangle, \tag{25c}$$

$$\rho_{eg'}(t) = \langle n_e l_e, \alpha_e J_e M_e|\hat{\rho}(t)|n'_g l'_g, \alpha_g J_g M_g\rangle. \tag{25d}$$

Here the diagonal elements $\rho_{gg}(t)$ and $\rho_{ee}(t)$ give the probability of finding the system in the states $|n_g l_g, \alpha_g J_g M_g\rangle$ and $|n_e l_e, \alpha_e J_e M_e\rangle$, respectively. At the same time, the off-diagonal elements describe the coherence between the states [71]. By using Eqs. (9) and (23)–(25), one obtains the following:

$$\frac{d}{dt}\rho_{gg'}(t) = -i\omega_{gg'}\,\rho_{gg'}(t) - \frac{i}{2\hbar}\sum_{n_e l_e}[(V_{ge}e^{-i\omega t} + V^\dagger_{ge}e^{i\omega t})\,\rho_{eg'}(t) - \rho_{ge}(t)(V_{eg'}e^{-i\omega t} + V^\dagger_{eg'}e^{i\omega t})], \tag{26a}$$

$$\frac{d}{dt}\rho_{ee'}(t) = -i\omega_{ee'}\,\rho_{ee'}(t) - \frac{i}{2\hbar}\sum_{n_g l_g}[(V_{eg}e^{-i\omega t} + V^\dagger_{eg}e^{i\omega t})\,\rho_{ge'}(t) - \rho_{eg}(t)(V_{ge'}e^{-i\omega t} + V^\dagger_{ge'}e^{i\omega t})], \tag{26b}$$

$$\frac{d}{dt}\rho_{ge}(t) = i\omega_{eg}\,\rho_{ge}(t) - \frac{i}{2\hbar}\left[\sum_{n'_e l'_e}(V_{ge'}e^{-i\omega t} + V^\dagger_{ge'}e^{i\omega t})\,\rho_{e'e}(t) - \sum_{n'_g l'_g}\rho_{gg'}(t)(V_{g'e}e^{-i\omega t} + V^\dagger_{g'e}e^{i\omega t})\right], \tag{26c}$$

$$\frac{d}{dt}\rho_{eg}(t) = -i\omega_{eg}\,\rho_{eg}(t) - \frac{i}{2\hbar}\left[\sum_{n'_g l'_g}(V_{eg'}e^{-i\omega t} + V^\dagger_{eg'}e^{i\omega t})\,\rho_{g'g}(t) - \sum_{n'_e l'_e}\rho_{ee'}(t)(V_{e'g}e^{-i\omega t} + V^\dagger_{e'g}e^{i\omega t})\right], \tag{26d}$$

where the transition matrix elements are

$$V_{eg} = \langle n_e l_e, \alpha_e J_e M_e|\hat{V}|n_g l_g, \alpha_g J_g M_g\rangle, \tag{27a}$$

$$V_{eg'} = \langle n_e l_e, \alpha_e J_e M_e|\hat{V}|n'_g l'_g, \alpha_g J_g M_g\rangle, \tag{27b}$$

$$V_{ge} = \langle n_g l_g, \alpha_g J_g M_g|\hat{V}|n_e l_e, \alpha_e J_e M_e\rangle, \tag{27c}$$

$$V_{ge'} = \langle n_g l_g, \alpha_g J_g M_g|\hat{V}|n'_e l'_e, \alpha_e J_e M_e\rangle. \tag{27d}$$

In Eqs. (26), ω_0 is the transition frequency for a free atom, whereas ω_{eg}, $\omega_{gg'}$, and $\omega_{ee'}$ are the frequencies of transitions in which vibrational states of a trapped atom change:

$$\omega_0 = (E_{\alpha_e J_e M_e} - E_{\alpha_g J_g M_g})/\hbar, \tag{28a}$$

$$\omega_{eg} = \omega_0 + \omega_r(2n_e + |l_e| - 2n_g - |l_g|), \tag{28b}$$

$$\omega_{gg'} = \omega_r(2n_g + |l_g| - 2n'_g - |l'_g|), \tag{28c}$$

$$\omega_{ee'} = \omega_r(2n_e + |l_e| - 2n'_e - |l'_e|). \tag{28d}$$

To eliminate the fast-oscillating terms in Eqs. (26), we follow the standard procedure and introduce the new variables:

$$\tilde{\rho}_{gg'}(t) = \rho_{gg'}(t), \tag{29a}$$

$$\tilde{\rho}_{ee'}(t) = \rho_{ee'}(t), \tag{29b}$$

$$\tilde{\rho}_{ge}(t) = \rho_{ge}(t)\, e^{-i\omega t}, \tag{29c}$$

$$\tilde{\rho}_{eg}(t) = \rho_{eg}(t)\, e^{i\omega t}. \tag{29d}$$

As seen from Eqs. (29), the density matrix elements $\tilde{\rho}_{ge}(t)$ and $\tilde{\rho}_{eg}(t)$, which characterize the interference between the ground and excited internal states, differ from their original counterparts $\rho_{ge}(t)$ and $\rho_{eg}(t)$ by a phase factor oscillating at the light frequency. At the same time, all other density matrix elements $\tilde{\rho}_{gg'}(t)$ and $\tilde{\rho}_{ee'}(t)$, including diagonal ones, are identical to the original $\rho_{gg'}(t)$ and $\rho_{ee'}(t)$. In fact, the transformation of the density matrix elements (29) is equivalent to using $|n_g l_g, \alpha_g J_g M_g\rangle$ and $|n_e l_e, \alpha_e J_e M_e\rangle e^{-i\omega t}$ as basis states. After substitution of Eqs. (29) into Eqs. (26), we employ the rotating-wave approximation in which fast-oscillating terms proportional to $e^{\pm i2\omega t}$ are neglected [72,73]. Hence,

$$\frac{d}{dt}\tilde{\rho}_{gg'}(t) = -i\omega_{gg'}\,\tilde{\rho}_{gg'}(t) - \frac{i}{2\hbar}\sum_{n_e l_e}[V^*_{eg}\,\tilde{\rho}_{eg'}(t) - \tilde{\rho}_{ge}(t)\,V_{eg'}], \tag{30a}$$

$$\frac{d}{dt}\tilde{\rho}_{ee'}(t) = -i\omega_{ee'}\,\tilde{\rho}_{ee'}(t) - \frac{i}{2\hbar}\sum_{n_g l_g}[V_{eg}\,\tilde{\rho}_{ge'}(t) - \tilde{\rho}_{eg}(t)V^*_{e'g}], \tag{30b}$$

$$\frac{d}{dt}\tilde{\rho}_{ge}(t) = -i(\omega - \omega_{eg})\,\tilde{\rho}_{ge}(t) - \frac{i}{2\hbar}\left[\sum_{n'_e l'_e} V^*_{e'g}\,\tilde{\rho}_{e'e}(t) - \sum_{n'_g l'_g}\tilde{\rho}_{gg'}(t)V^*_{eg'}\right], \tag{30c}$$

$$\frac{d}{dt}\tilde{\rho}_{eg}(t) = i(\omega - \omega_{eg})\,\tilde{\rho}_{eg}(t) - \frac{i}{2\hbar}\left[\sum_{n'_g l'_g} V_{eg'}\,\tilde{\rho}_{g'g}(t) - \sum_{n'_e l'_e}\tilde{\rho}_{ee'}(t)\,V_{e'g}\right], \tag{30d}$$

where we have made use of the relation $V^\dagger_{ge} = V^*_{eg}$. Because of the absence of time-dependent exponential factors, the system of Eqs. (30) is much simpler than the original system (26).

D. Evaluation of the transition matrix element

In order to solve Eqs. (30), one needs to evaluate the matrix element V_{eg} for the $|n_g l_g, \alpha_g J_g M_g\rangle + \gamma \to |n_e l_e, \alpha_e J_e M_e\rangle$ transition. It involves internal and center-of-mass wave functions and may be written as

$$V_{eg} = \langle n_e l_e, \alpha_e J_e M_e|\hat{V}|n_g l_g, \alpha_g J_g M_g\rangle = \int U^*_{n_e l_e}(\boldsymbol{R}_\perp)\,\mathcal{M}^{(\mathrm{tw})}_{M_e M_g}(\boldsymbol{R}_\perp)\,U_{n_g l_g}(\boldsymbol{R}_\perp)\,d^2\boldsymbol{R}_\perp, \tag{31}$$

where

$$\mathcal{M}^{(\mathrm{tw})}_{M_e M_g}(\boldsymbol{R}_\perp) = -\frac{i\hbar e}{\mathfrak{m}_e}\int \psi^*_{\alpha_e J_e M_e}(\boldsymbol{r}) \times \boldsymbol{A}^{(\mathrm{tw})}(\boldsymbol{r}+\boldsymbol{R}_\perp)\cdot\nabla_r\,\psi_{\alpha_g J_g M_g}(\boldsymbol{r})\,d\boldsymbol{r} \tag{32}$$

is the matrix element for the transition between internal electronic levels. For inhomogeneous LG modes, $\mathcal{M}^{(\mathrm{tw})}_{M_e M_g}$ depends on the atomic center-of-mass coordinate $\boldsymbol{R}_\perp$.

By means of the vector potential (10), we can express the "electronic" matrix element

$$\mathcal{M}^{(\mathrm{tw})}_{M_e M_g}(\boldsymbol{R}_\perp) = A_0\int a_m(k_\perp) \times e^{i(m+\lambda)\phi_k + i\boldsymbol{k}_\perp\boldsymbol{R}_\perp}\,\mathcal{M}^{(\mathrm{pl})}_{M_e M_g}(\theta_k,\phi_k)\,\frac{d^2\boldsymbol{k}_\perp}{2\pi} \tag{33}$$

in terms of its well-known plane-wave counterpart

$$\mathcal{M}^{(\mathrm{pl})}_{M_e M_g}(\theta_k,\phi_k) = -\frac{i\hbar e}{\mathfrak{m}_e}\int \psi^*_{\alpha_e J_e M_e}(\boldsymbol{r}) \times \boldsymbol{e}_{\boldsymbol{k}\lambda}\,e^{i\boldsymbol{k}\boldsymbol{r}}\cdot\nabla_r\,\psi_{\alpha_g J_g M_g}(\boldsymbol{r})\,d\boldsymbol{r}. \tag{34}$$

Since the evaluation of $\mathcal{M}^{(\mathrm{pl})}_{M_e M_g}$ has been often discussed in the literature [31,41], we indicate only its main steps. One usually employs the multipole expansion of the plane wave,

$$\boldsymbol{e}_{\boldsymbol{k}\lambda}\,e^{i\boldsymbol{k}\boldsymbol{r}} = \sqrt{2\pi}\sum_{LM}\sum_{p=0,1} i^L[L]^{1/2}\,(i\lambda)^p \times D^L_{M\lambda}(\phi_k,\theta_k,0)\,\boldsymbol{a}^{(p)}_{LM}(\boldsymbol{r}), \tag{35}$$

for arbitrary propagation direction $\hat{\boldsymbol{k}} = \boldsymbol{k}/k = (\theta_k,\phi_k)$. Here $[L] = 2L+1$, $D^L_{M\lambda}(\phi_k,\theta_k,0) = e^{-iM\phi_k}d^L_{M\lambda}(\theta_k)$ stands for the Wigner D function, and $\boldsymbol{a}^{(p)}_{LM}(\boldsymbol{r})$ refers to magnetic ($p=0$) and electric ($p=1$) multipole components [67]. The important feature of $\boldsymbol{a}^{(p)}_{LM}(\boldsymbol{r})$ is that they are constructed as irreducible tensors of rank L. Inserting the expansion (35) into Eq. (34) and making use of the Wigner-Eckart theorem, we obtain

$$\mathcal{M}^{(\mathrm{pl})}_{M_e M_g}(\theta_k,\phi_k) = ec\sqrt{2\pi}\sum_{Lp} i^L\frac{[L]^{1/2}}{[J_e]^{1/2}}\,(i\lambda)^p\,D^L_{M_e-M_g,\lambda}(\phi_k,\theta_k,0) \times \langle J_g M_g\, LM_e - M_g|J_e M_e\rangle\,\langle\alpha_e J_e||H_\gamma(pL)||\alpha_g J_g\rangle, \tag{36}$$

where the reduced matrix element $\langle\alpha_e J_e||H_\gamma(pL)||\alpha_g J_g\rangle$ reflects the electronic structure of an atom and is independent of the projections of its angular momentum.

The multipole expansion of the electronic matrix element allows one to further simplify $\mathcal{M}^{(\mathrm{tw})}_{M_e M_g}$. Indeed, if we substitute

Eq. (36) into Eq. (33) and integrate over ϕ_k, we find that

$$\mathcal{M}^{(\mathrm{tw})}_{M_e M_g}(\boldsymbol{R}_\perp) = e^{i(m+\lambda+M_g-M_e)\Phi}\,\mathcal{M}^{(\mathrm{tw})}_{M_e M_g}(R_\perp). \tag{37}$$

In this expression Φ is the azimuthal angle of $\boldsymbol{R}_\perp$ and

$$\begin{aligned}\mathcal{M}^{(\mathrm{tw})}_{M_e M_g}(R_\perp) = ecA_0\sqrt{2\pi}\sum_{Lp} i^L\,\frac{[L]^{1/2}}{[J_e]^{1/2}}\,(i\lambda)^p \\ \times\, i^{m+\lambda+M_g-M_e}\,\langle J_g M_g\, LM_e - M_g | J_e M_e\rangle \\ \times\, \langle \alpha_e J_e||H_\gamma(pL)||\alpha_g J_g\rangle \int_0^\infty a_m(k_\perp) \\ \times\, d^L_{M_e-M_g,\,\lambda}(\theta_k)\, J_{m+\lambda+M_g-M_e}(k_\perp R_\perp)\, k_\perp\, dk_\perp.\end{aligned} \tag{38}$$

With the help of Eqs. (37) and (38), we finally obtain the transition matrix element:

$$\begin{aligned}V_{eg} = 2\pi\,\delta_{m+\lambda+M_g+l_g,\,M_e+l_e} \\ \times \int_0^\infty u^*_{n_e l_e}(R_\perp)\,\mathcal{M}^{(\mathrm{tw})}_{M_e M_g}(R_\perp)\,u_{n_g l_g}(R_\perp)\,R_\perp\,dR_\perp,\end{aligned} \tag{39}$$

where we have performed the integration over Φ and used the first line of Eq. (5). The Kronecker symbol in Eq. (39) reflects the selection rule:

$$m + \lambda + M_g + l_g = M_e + l_e, \tag{40}$$

which connects the angular momentum projections of an atom with those of photons [45]. This selection rule is valid for the case when the quantization axis is parallel to the light propagation direction and the beam center coincides with the equilibrium point of the trap. If this condition is not satisfied, Eq. (40) breaks down and twisted light may potentially couple all possible angular momentum states of atomic motion.

III. RESULTS AND DISCUSSION

After inserting the transition matrix element (39) into a system of coupled differential equations (30), we can calculate the time evolution of the atomic density matrix. As an example, we consider the excitation of a single trapped $^{40}Ca^+$ ion that is initially prepared in the $M_g = -1/2$ magnetic sublevel of the $4s\ ^2S_{1/2}$ ground electronic state. Moreover, the ion's motion is initially cooled to the lowest vibrational state of the trap, which is characterized by the quantum numbers $n_g = l_g = 0$. The trapping frequency is chosen to be $\omega_\mathrm{r} = 2\pi \times 10\,\mathrm{kHz}$, which is much smaller than the frequency of a typical atomic transition. In what follows we examine the transition $4s\ ^2S_{1/2} \to 3d\ ^2D_{5/2}$ with frequency $\omega_0 = 2\pi \times 411$ THz induced by a LG_{0m} laser mode with helicity $\lambda = +1$ and OAM $m = +1$. Of particular interest here are $|\,^2S_{1/2}\ M_g = -1/2\rangle + \gamma \to |\,^2D_{5/2}\ M_e = +1/2\rangle$ and $|\,^2S_{1/2}\ M_g = -1/2\rangle + \gamma \to |\,^2D_{5/2}\,M_e = +3/2\rangle$ electronic transitions, which can be excited separately due to the Zeeman effect in an applied magnetic field. These transitions, which proceed predominantly via the $E2$ channel, have already been employed to demonstrate the transfer of optical OAM to a bound atomic electron [30]. The beam waist is taken to be $w_0 = 2.7\ \mu$m. For comparison, the characteristic width of the harmonic-oscillator ground-state wave function for $^{40}Ca^+$ is $b = 159$ nm.

As seen from Eqs. (38) and (39), one needs to know the reduced matrix element for the chosen transition, $\langle 3d\ ^2D_{5/2}\,||H_\gamma(E2)||4s\ ^2S_{1/2}\rangle$, in order to solve the system of Eqs. (30). In our work, this matrix element is obtained from the relation

$$\left\langle 3d\,^2D_{5/2}||H_\gamma(E2)||4s\,^2S_{1/2}\right\rangle = \sqrt{\frac{6}{8\pi\alpha\omega_0\tau}} \tag{41}$$

for the natural lifetime $\tau = 1.163\,\mathrm{s}$ of the $3d\ ^2D_{5/2}$ excited state [74–76], and where α is the fine-structure constant. Apart from the reduced matrix element, one must determine the size of the basis $|nl, \alpha JM\rangle$ to be used in computations. In addition to two atom's internal levels coupled by an optical field, we take into account all its vibrational levels with $2n + |l| \leqslant 6$. This results in the 28 harmonic oscillator states for both the ground and the excited electronic states. A set of 3136 coupled differential equations must then be solved numerically to obtain the time evolution of the density matrix. The size of the basis has been determined based on convergence analysis. The validity of this approach is confirmed by the agreement with the results obtained by solving numerically the two-dimensional Schrödinger equation.

A. Rabi oscillations between the internal states

One of the most common observables in light-atom interaction experiments is the probability $p_e(t)$ for finding an atom in an upper electronic state. In our density matrix approach, this probability is found by summing over the vibrational levels:

$$p_e(t) = \sum_{n_e, l_e} \tilde{\rho}_{ee}(t). \tag{42}$$

The upper panels of Fig. 3 show the time evolution of the population (42) for the case of the $M_g = -1/2 \to M_e = +3/2$ transition and for two light powers, $P = 1\ \mu$W and $20\ \mu$W. Moreover, $p_e(t)$ is calculated for different frequencies of incident light, characterized by the detuning $\delta = \omega - \omega_0$. This parameter is defined as the difference between the radiation frequency ω and the transition frequency ω_0 for a free atom. The results are presented in Fig. 3 for $\delta = 0$ (red solid lines) and $\delta = \omega_\mathrm{r}$ (blue dashed lines). As expected, the excited-state population $p_e(t)$ shows a clear oscillatory behavior, referred to as Rabi flopping [7]. For nonzero detuning $\delta \neq 0$, as is well known, the amplitude of Rabi oscillations is reduced but their frequency is enhanced. The latter can be seen from the frequency spectrum of $p_e(t)$ presented in the bottom panels of Fig. 3. It is also apparent that the Rabi flopping frequency increases with light intensity.

Compared to the $M_g = -1/2 \to M_e = +3/2$ case, $p_e(t)$ for the $M_g = -1/2 \to M_e = +1/2$ transition exhibits qualitatively different behavior (see Fig. 4). In particular, the amplitude of Rabi oscillations increases as the light is tuned away from $\delta = 0$. For low-intensity $P = 1\ \mu$W, complete population transfer, $\max(p_e) = 1$, is achieved when $\delta = \omega_\mathrm{r}$. Moreover, a remarkable anharmonicity of Rabi flopping is observed at higher light power, $P = 20\ \mu$W. The origin of such complex population dynamics lies in the excitation of the atomic center-of-mass motion accompanied by the transfer of angular momentum. This aspect is discussed in detail below.

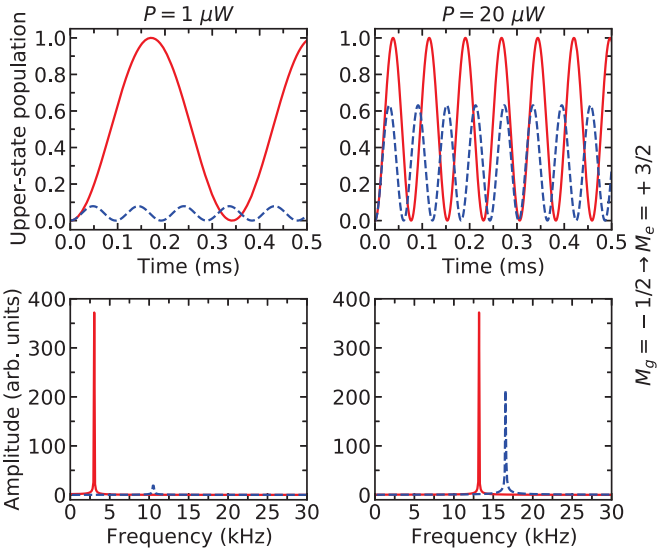

FIG. 3. Top: Population (42) of the $M_e = +3/2$ excited magnetic sublevel of $^{40}Ca^+$ as a function of time. Calculations have been performed for the $M_g = -1/2 \rightarrow M_e = +3/2$ transition induced by a LG_{0m} beam with helicity $\lambda = +1$ and OAM $m = +1$. Here, the beam waist is $w_0 = 2.7$ μm, and the total power is $P = 1$ μW or 20 μW. Rabi oscillations for the light frequency detuning $\delta = 0$ (red solid lines) are compared with those for $\delta = \omega_r$ (blue dashed lines), while the trapping frequency is $\omega_r = 2\pi \times 10$ kHz. Bottom: Corresponding Fourier spectrum of the Rabi oscillations.

B. Excitation of the center-of-mass motion

To better understand how the Rabi oscillations are affected by the atomic motion in the trap, we employed two different models to calculate the population $p_e(t)$. In the first model, which was already used above, all vibrational states with $2n + |l| \leqslant 6$ are taken into account. The corresponding results are displayed by red solid lines in the upper panels of Figs. 5 and 6. In the second model, whose predictions are depicted

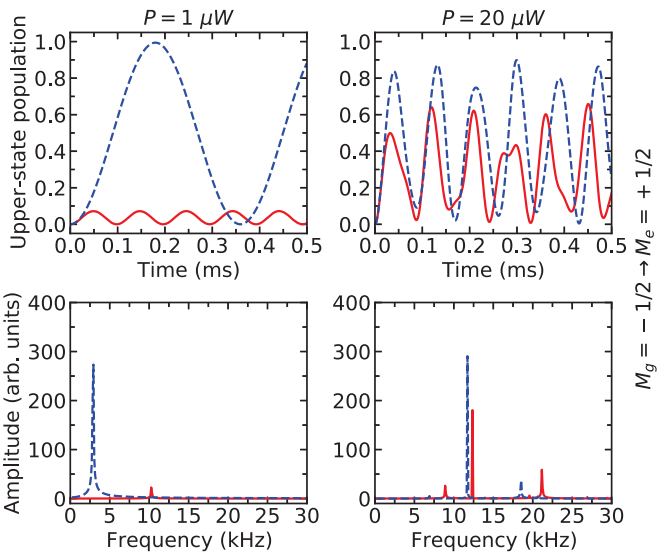

FIG. 4. Same as Fig. 3, but for the $M_e = +1/2$ magnetic sublevel of $^{40}Ca^+$ in the case of the $M_g = -1/2 \rightarrow M_e = +1/2$ transition.

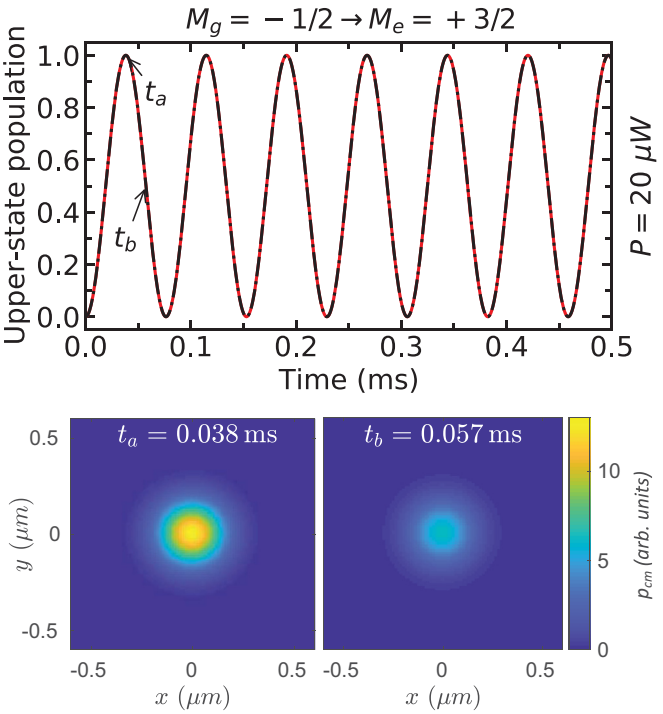

FIG. 5. Top: Probability (42) for finding $^{40}Ca^+$ in the $M_e = +3/2$ upper magnetic sublevel as a function of time. Results are presented for the $M_g = -1/2 \rightarrow M_e = +3/2$ transition by including (red solid line) or neglecting (black dash-dotted line) excited vibrational states. The total power of the beam is $P = 20$ μW, and its frequency detuning is $\delta = 0$. All other beam and trap parameters are the same as those in Fig. 3. Bottom: Corresponding center-of-mass probability distribution p_{cm} (arb. units) for the ion in the $M_e = +3/2$ excited sublevel at two different times.

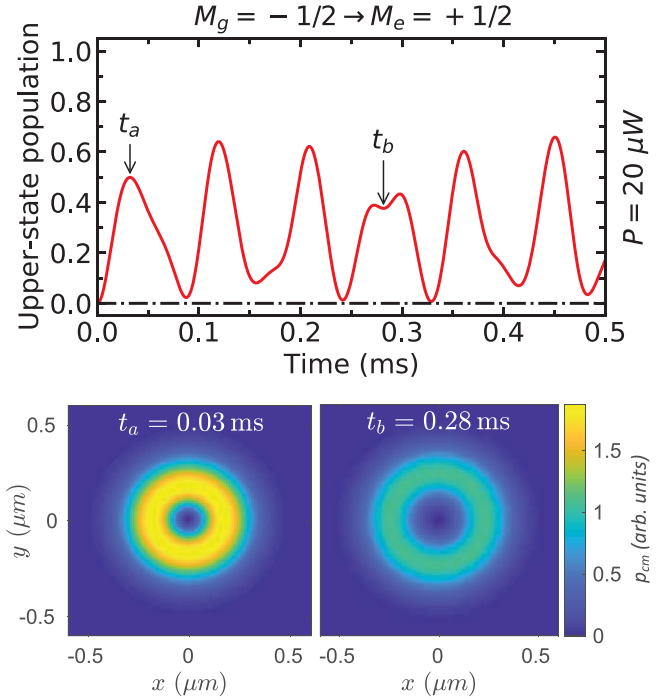

FIG. 6. Same as Fig. 5, but for the $M_e = +1/2$ magnetic sublevel of $^{40}Ca^+$ in the case of the $M_g = -1/2 \rightarrow M_e = +1/2$ transition.

by black dash-dotted lines, we "forbid" excitations of the center-of-mass motion by restricting the basis of harmonic oscillator states to the ground one $|n_g = l_g = 0\rangle$. For the case of the $M_g = -1/2 \to M_e = +3/2$ transition, shown in Fig. 5, both models predict the same behavior of $p_e(t)$, thus clearly indicating that the atom remains in the lowest vibrational state of the trap at any instant of time. The latter is also illustrated in the bottom panel of Fig. 5, which shows the center-of-mass probability distribution for the ion in the $M_e = +3/2$ excited sublevel. Indeed, the excited atom stays localized at the trap's center according to the ground-state (Gaussian) distribution.

The absence of vibrational excitations observed in Fig. 5 can be explained by the conservation of the total angular momentum (TAM) projection. Namely, for the $M_g = -1/2 \to M_e = +3/2$ transition, the TAM projection of light $m + \lambda = 1 + 1$ is completely transferred to the bound atomic electron, i.e., $M_e - M_g = m + \lambda$. The selection rule (40) then dictates that $l_e = l_g$ and, hence, no transfer of angular momentum to the atomic motion occurs. Moreover, the transitions with $n_e \neq n_g$ are strongly suppressed for paraxial light beams and for the ion localized near the beam's center. Under these conditions $k_\perp R_\perp \to 0$, and the Bessel function $J_0(k_\perp R_\perp)$ in Eq. (38) can be approximated by unity. This implies that $\mathcal{M}^{(\mathrm{tw})}_{M_e M_g}$ is a constant, and the integral over $\boldsymbol{R}_\perp$ in the matrix element (31) reduces to the orthogonality relation $\langle n_e l_e | n_g l_g \rangle = \delta_{n_e n_g}\, \delta_{l_e l_g}$. It clearly indicates that the $M_g = -1/2 \to M_e = +3/2$ transition proceeds without excitation of the center-of-mass motion, and therefore a resonance in the Rabi oscillations is achieved when $\delta = \omega - \omega_0 = 0$.

In the case when $M_e - M_g < m + \lambda$, only a part of the TAM projection is transferred to internal degrees of freedom, and the excitation of atomic motion is no longer negligible. This effect can be seen from Rabi oscillations between the $M_g = -1/2$ and $M_e = +1/2$ magnetic sublevels. As displayed by the black dash-dotted line in Fig. 6, the exclusion of high-lying vibrational states results in the complete absence of population of the $M_e = +1/2$ excited electronic sublevel. In contrast, the "rigorous" calculations (red solid line) demonstrate the presence of Rabi oscillations, which, however, deviate significantly from an ideal sinusoidal pattern. The observed oscillations are essentially a manifestation of transitions accompanied by the transfer of one unit of angular momentum projection to the center-of-mass motion, $l_e = l_g + 1$ [45,46]. The necessity of this transfer follows from the general selection rule (40) and has two important consequences. First, the center-of-mass probability distribution for the atom in the $M_e = +1/2$ sublevel exhibits an annular shape, which is typical for the $l_e = 1$ state (see the bottom panels of Fig. 6). Second, the condition $l_e = l_g + 1$ implies a gain or loss of energy in the transition between vibrational levels. This means that the resonance in Rabi flopping is achieved when the frequency of radiation does not precisely coincide with the atomic transition frequency. Indeed, as seen from Fig. 4, the amplitude of Rabi oscillations reaches its maximum at $\delta = \omega_\mathrm{r}$.

C. Anharmonic Rabi oscillations

Although angular momentum conservation (40) explains why Rabi oscillations for the $M_g = -1/2 \to M_e = +1/2$ transition become amplified in the detuned regime $\delta = \omega_\mathrm{r}$, it does not provide clear insight into the observed anharmonic population dynamics (see Fig. 4). This anharmonicity can be attributed to the excitation of vibrational states with different quantum numbers n_g and n_e during the interaction with twisted light. In order to determine which states n_g and n_e are coupled to each other, we must revisit the matrix element (31). It consists of two important "ingredients": the electronic matrix element $\mathcal{M}^{(\mathrm{tw})}_{M_e M_g}$ and the harmonic oscillator wave functions (5). We start with $\mathcal{M}^{(\mathrm{tw})}_{M_e M_g}$ and use the identity $l_e = l_g + 1$, together with the fact that the center-of-mass wave function is localized close to the beam center. In this case, $J_1(k_\perp R_\perp) \approx k_\perp R_\perp/2$ and the matrix element (37) can be simplified to

$$\mathcal{M}^{(\mathrm{tw})}_{M_e M_g}(\boldsymbol{R}_\perp) \approx N R_\perp e^{i\Phi}, \tag{43}$$

where the constant N is determined by the atomic properties and the light intensity. For the harmonic oscillator wave functions, in turn, we can establish the three-point rules

$$\begin{aligned} R_\perp e^{i\Phi} U_{n,l}(\boldsymbol{R}_\perp) &= b[\sqrt{n+l+1}\, U_{n,l+1}(\boldsymbol{R}_\perp) \\ &\quad - \sqrt{n}\, U_{n-1,l+1}(\boldsymbol{R}_\perp)], \\ R_\perp e^{-i\Phi} U_{n,l}(\boldsymbol{R}_\perp) &= b[\sqrt{n+l}\, U_{n,l-1}(\boldsymbol{R}_\perp) \\ &\quad - \sqrt{n+1}\, U_{n+1,l-1}(\boldsymbol{R}_\perp)], \end{aligned} \tag{44}$$

based on the recurrence relations for associated Laguerre polynomials [77] and assuming positive values of angular momentum quantum numbers l_g and l_e. By combining Eqs. (43) and (44) we obtain a simple expression for the matrix element (31) for the case of the $M_e - M_g = +1$ excitation:

$$\begin{aligned} V_{eg} &\approx N \int U^*_{n_e l_e}(\boldsymbol{R}_\perp) R_\perp e^{i\Phi} U_{n_g l_g}(\boldsymbol{R}_\perp)\, d^2\boldsymbol{R}_\perp \\ &= Nb\big[\sqrt{n_g + l_g + 1}\, \delta_{n_e, n_g} - \sqrt{n_g}\, \delta_{n_e, n_g - 1}\big] \delta_{l_e, l_g + 1}. \end{aligned} \tag{45}$$

From the above formula one sees that transitions proceed not only between vibrational levels with $n_e = n_g$ but also between $n_e = n_g - 1$. This suggests that even though the system is initially in the ground state $n_g = 0$, the interaction between an atom and twisted light leads to the population of high-lying vibrational states with n_e and l_e greater than zero, an effect which can be seen as heating. Such a redistribution of vibrational levels, and corresponding $|n_g l_g\rangle + \gamma \to |n_e l_e\rangle$ sideband transitions, results in the anharmonicity of the internal-state population dynamics. It is reasonable to expect [61] that the Rabi frequencies for these transitions are given by

$$\begin{aligned} \Omega &= \sqrt{\Omega_\mathrm{R}^2 + [\delta + \omega_0 - \omega_{eg}]^2} \\ &= \sqrt{\Omega_\mathrm{R}^2 + [\delta - (2n_e + |l_e| - 2n_g - |l_g|)\, \omega_\mathrm{r}]^2}, \end{aligned} \tag{46}$$

where the resonant Rabi frequency is defined according to

$$\Omega_\mathrm{R} = \frac{|V_{eg}|}{\hbar} = \frac{1}{\hbar} |\langle n_e l_e, \alpha_e J_e M_e | \hat{V} | n_g l_g, \alpha_g J_g M_g \rangle|. \tag{47}$$

To assess the validity of the formula (46), we compare its predictions with the results of Fourier analysis of the excited-state population oscillations $p_e(t)$. The spectra obtained within these two—analytical and numerical—approaches are

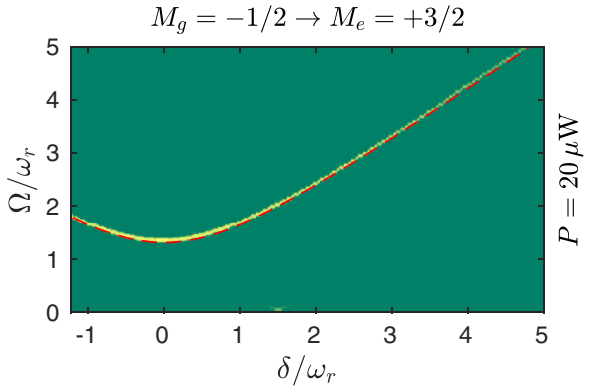

FIG. 7. Fourier spectrum of Rabi oscillations, calculated with different values of frequency detuning δ, for the transition $M_g = -1/2 \to M_e = +3/2$ and the total beam power $P = 20$ μW. The background color represents the calculated spectral density [low in dark green (dark gray), high in light yellow (light gray)], while the red (black) dashed line displays the analytical prediction (46) for vibrational quantum numbers $l_g = l_e = 0$ and $n_g = n_e = 0$. All other parameters are the same as those in Fig. 3.

presented as a function of the detuning parameter δ for the two electronic transitions $M_g = -1/2 \to M_e = +3/2$ and $M_g = -1/2 \to M_e = +1/2$ in Figs. 7 and 8, respectively. It is apparent from Fig. 7 that the numerically obtained single-frequency spectrum for the excitation of the $M_e = +3/2$ sublevel is accurately reproduced by Eq. (46) with $l_g = l_e = 0$ and $n_g = n_e = 0$. In particular, as mentioned above, the lowest frequency Ω is achieved at zero detuning $\delta = 0$ and no sideband lines appear. In contrast to this textbook example, the spectrum of Rabi oscillations between $M_g = -1/2$ and $M_e = +1/2$ sublevels contains several peaks at any detuning parameter δ (see Fig. 8). For low-intensity $P = 1$ μW, the formula (46) allows us to attribute these peaks to transitions between vibrational states with $l_e = l_g + 1 = 1$ and $n_g = n_e = 0$ [red (black) lines], $n_g = 1$ and $n_e = 0$ (white lines), and $n_g = 0$ and $n_e = 1$ [blue (gray) lines], which make the main contribution to the atomic dynamics. Moreover, the high brightness of the numerical result associated with the red dashed line indicates that the $n_g = n_e = 0$ carrier transition is dominant in the low-intensity limit. Herewith the sideband transitions are so weak that they are not even visible in Fig. 4.

With increasing light intensity, the spectrum of Rabi oscillations departs more and more from the behavior predicted by Eq. (46). This effect is shown in the lower panels of Fig. 8 and can be attributed to the "heating" of the system, which begins at about 0.02 ms for our set of parameters. Indeed, the redistribution of an atom over many high-lying vibrational states makes the identification of a specific sideband (or carrier) transition unattainable and leads to the breakdown of the approximation (46). In order to determine the range of intensities for which the formula (46) is still valid, we display in Fig. 9 the Fourier spectrum of $p_e(t)$ for the $M_e = +1/2$ state as a function of (the square root of) the total beam power P. In the particular case of a detuning $\delta = \omega_r$, light is resonant with the $|M_g = -1/2,\ n_g = 0,\ l_g = 0\rangle + \gamma \to |M_e = +1/2,\ n_e = 0,\ l_e = 1\rangle$ transition for which a single major peak in the spectrum of Rabi oscillations at the frequency $\Omega = \Omega_R$ should

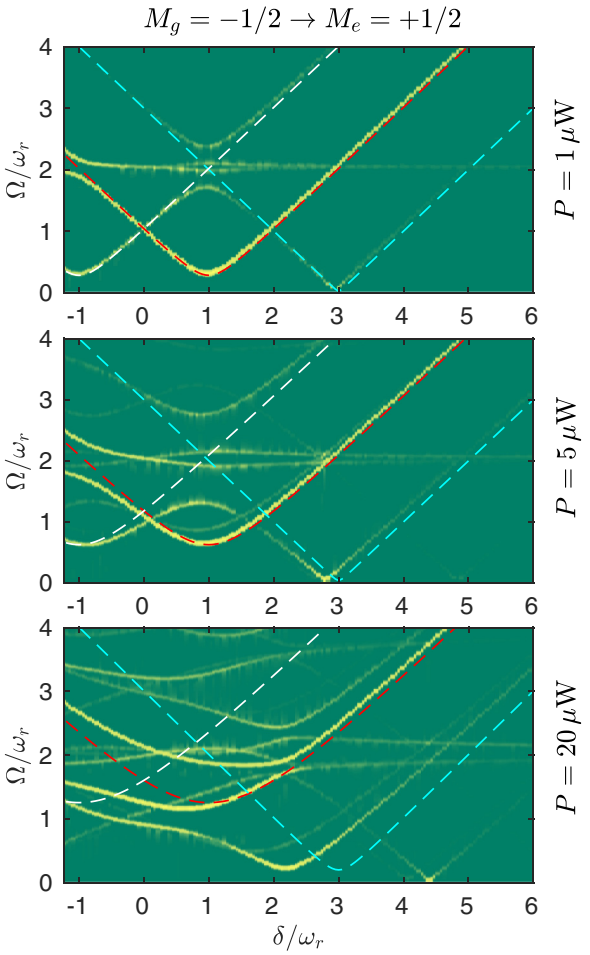

FIG. 8. Same as Fig. 7, but for the $M_g = -1/2 \to M_e = +1/2$ transition. The spectral densities were computed for three different total beam powers: $P = 1$ μW (upper panel), 5 μW (middle panel), and 20 μW (bottom panel). The dashed lines display analytical predictions (46) for vibrational quantum numbers $n_g = n_e = 0$ [red (black)], $n_g = 1$, $n_e = 0$ (white), and $n_g = 0$, $n_e = 1$ [blue (gray)]. In all cases, $l_g = 0$ and $l_e = 1$.

appear according to Eq. (46). Since the resonant Rabi frequency is proportional to the transition matrix element, and hence to the electric field [cf. Eq. (19)], one can expect that $\Omega \propto \sqrt{P}$. As seen from the figure, this dependence (red solid line) holds well up to the critical power $P \approx 12$ μW. For higher intensities, it breaks down and, moreover, additional lines appear in the spectrum. It should be noted that at the critical power $P \approx 12$ μW the Rabi frequency Ω_R becomes comparable to the trapping frequency ω_r, which is depicted by the blue horizontal line in Fig. 9. In this regime the coupling of an atom to twisted light leads to a transfer not only of angular momentum but also of energy to the atom's center-of-mass motion. This effect is different from sideband laser cooling (or heating) [61] in that no dissipation in the form of spontaneous photon emission is taking place.

IV. SUMMARY AND OUTLOOK

In summary, we have presented a theoretical investigation of the excitation of a single trapped atom by twisted light.

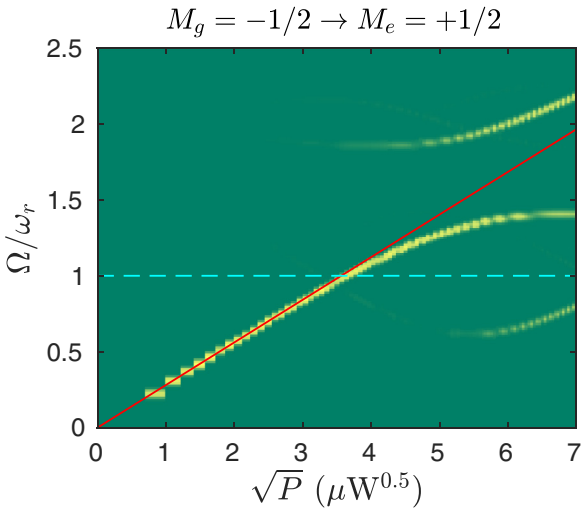

FIG. 9. Fourier spectrum of the Rabi oscillations (42) between states $M_g = -1/2$ and $M_e = +1/2$ versus (the square root of) the total beam power P for the radiation's frequency detuning $\delta = \omega_r$. The red solid line corresponds to the resonant Rabi frequency (47) for vibrational quantum numbers $l_g = 0$, $l_e = 1$, and $n_g = n_e = 0$, whereas the blue dashed line marks the trapping frequency ω_r for comparison. All other parameters are the same as those in Fig. 3.

Emphasis has been placed on the interplay of the atom's internal-state population dynamics and the center-of-mass motion. In order to explore the evolution of such a complex system with many degrees of freedom, we have employed the density matrix formalism based on the Liouville–von Neumann equation. Although the approach developed here is universal and can be used to describe the photoexcitation of any atom, calculations have been performed for the $4s\ ^2S_{1/2} \rightarrow 3d\ ^2D_{5/2}$ transition in the $^{40}Ca^+$ ion. We have shown that the angular momentum transfer from twisted light to the atomic center-of-mass motion can lead to unconventional behavior of Rabi oscillations. In particular, the anharmonic time evolution of the internal-state population has been observed and attributed to the redistribution of an atom over many vibrational states. This anharmonicity was found to be most pronounced when the Rabi oscillation frequency Ω_R was comparable to or larger than the trapping frequency ω_r. In the opposite case $\Omega_R \ll \omega_r$, we have observed the conventional harmonic Rabi flopping, for which the complete population transfer is achieved if the light frequency is shifted by an integer number of trapping frequencies. These findings reveal the importance of quantum motion effects in experiments on the interaction of atoms with twisted-light modes. In particular, we conclude that the use of twisted light in atomic spectroscopy based on controllable measurements of the Rabi flopping frequency is feasible only if $\Omega_R \ll \omega_r$. While we present results for a selected trapping frequency $\omega_r = 2\pi \times 10\,\mathrm{kHz}$, our calculations, as well as Eq. (45), indicate that similar predictions can be obtained for a trapping frequency of $\chi \cdot \omega_r$ and an adjusted beam power of $\chi^3 \cdot P$.

The present study was restricted to an atom which is initially prepared in the lowest vibrational state of the trap. Future experiments, however, are likely to be performed with some initial distribution of vibrational state population. This circumstance, together with the spontaneous emission mechanism, may result in additional anharmonicity phenomena in Rabi oscillations and affect sideband cooling protocols. An analysis of these effects based on the developed theory is currently under way and will be presented in a forthcoming publication.

ACKNOWLEDGMENTS

This work was funded by the Deutsche Forschungsgemeinschaft (DFG, German Research Foundation) under Project-ID 445408588 (SU 658/5-1) and Project-ID 274200144, under SFB 1227 within project B02, and under Germany's Excellence Strategy, EXC-2123 QuantumFrontiers, Project No. 390837967.

[1] A. D. Ludlow, M. M. Boyd, J. Ye, E. Peik, and P. O. Schmidt, Rev. Mod. Phys. **87**, 637 (2015).
[2] M. S. Safronova, D. Budker, D. DeMille, D. F. Jackson Kimball, A. Derevianko, and C. W. Clark, Rev. Mod. Phys. **90**, 025008 (2018).
[3] R. Lange, N. Huntemann, J. M. Rahm, C. Sanner, H. Shao, B. Lipphardt, Chr. Tamm, S. Weyers, and E. Peik, Phys. Rev. Lett. **126**, 011102 (2021).
[4] H. Häffner, C. F. Roos, and R. Blatt, Phys. Rep. **469**, 155 (2008).
[5] T. E. Mehlstäubler, G. Grosche, C. Lisdat, P. O. Schmidt, and H. Denker, Rep. Prog. Phys. **81**, 064401 (2018).
[6] H. Müller, A. Peters, and S. Chu, Nature (London) **463**, 926 (2010).
[7] M. Fox, *Quantum Optics: An Introduction* (Oxford University, Oxford, 2006).
[8] D. Leibfried, R. Blatt, C. Monroe, and D. Wineland, Rev. Mod. Phys. **75**, 281 (2003).
[9] J. Eschner, G. Morigi, F. Schmidt-Kaler, and R. Blatt, J. Opt. Soc. Am. B **20**, 1003 (2003).
[10] A. E. Siegman, *Lasers* (University Science Books, Mill Valley, CA, 1986).
[11] L. Allen, M. W. Beijersbergen, R. J. C. Spreeuw, and J. P. Woerdman, Phys. Rev. A **45**, 8185 (1992).
[12] G. J. Gbur, *Singular Optics* (CRC, Boca Raton, FL, 2017).
[13] M. Erhard, R. Fickler, M. Krenn, and A. Zeilinger, Light Sci. Appl. **7**, 17146 (2018).
[14] B. A. Knyazev and V. G. Serbo, Phys.-Usp. **61**, 449 (2018).
[15] F. Castellucci, T. W. Clark, A. Selyem, J. Wang, and S. Franke-Arnold, Phys. Rev. Lett. **127**, 233202 (2021).
[16] Y. Shen, X. Wang, Z. Xie, C. Min, X. Fu, Q. Liu, M. Gong, and X. Yuan, Light: Sci. Appl. **8**, 90 (2019).
[17] K. Bongs, S. Burger, S. Dettmer, D. Hellweg, J. Arlt, W. Ertmer, and K. Sengstock, Phys. Rev. A **63**, 031602(R) (2001).
[18] M. Bhattacharya, Opt. Commun. **279**, 219 (2007).
[19] V. Carrat, C. Cabrera-Gutiérrez, M. Jacquey, J. W. Tabosa, B. Viaris de Lesegno, and L. Pruvost, Opt. Lett. **39**, 719 (2014).
[20] S. E. Olson, M. L. Terraciano, M. Bashkansky, and F. K. Fatemi, Phys. Rev. A **76**, 061404(R) (2007).
[21] P. Xu, X. He, J. Wang, and M. Zhan, Opt. Lett. **35**, 2164 (2010).

[22] S. A. Kennedy, G. W. Biedermann, J. T. Farrar, T. G. Akin, S. P. Krzyzewski, and E. R. I. Abraham, Opt. Commun. **321**, 110 (2014).

[23] R. Pugatch, M. Shuker, O. Firstenberg, A. Ron, and N. Davidson, Phys. Rev. Lett. **98**, 203601 (2007).

[24] D. Moretti, D. Felinto, and J. W. R. Tabosa, Phys. Rev. A **79**, 023825 (2009).

[25] S. Franke-Arnold, Philos. Trans. R. Soc., A **375**, 20150435 (2017).

[26] M. Drechsler, S. Wolf, C. T. Schmiegelow, and F. Schmidt-Kaler, Phys. Rev. Lett. **127**, 143602 (2021).

[27] S. Gröblacher, T. Jennewein, A. Vaziri, G. Weihs, and A. Zeilinger, New J. Phys. **8**, 75 (2006).

[28] G. Molina-Terriza, J. P. Torres, and L. Torner, Nat. Phys. **3**, 305 (2007).

[29] A. Sit, F. Bouchard, R. Fickler, J. Gagnon-Bischoff, H. Larocque, K. Heshami, D. Elser, C. Peuntinger, K. Günthner, B. Heim, C. Marquardt, G. Leuchs, R. W. Boyd, and E. Karimi, Optica **4**, 1006 (2017).

[30] C. T. Schmiegelow, J. Schulz, H. Kaufmann, T. Ruster, U. G. Poschinger, and F. Schmidt-Kaler, Nat. Commun. **7**, 12998 (2016).

[31] S. A.-L. Schulz, A. A. Peshkov, R. A. Müller, R. Lange, N. Huntemann, Chr. Tamm, E. Peik, and A. Surzhykov, Phys. Rev. A **102**, 012812 (2020).

[32] A. Picón, A. Benseny, J. Mompart, J. R. Vázquez de Aldana, L. Plaja, G. F. Calvo, and L. Roso, New J. Phys. **12**, 083053 (2010).

[33] K. Köksal and J. Berakdar, Phys. Rev. A **86**, 063812 (2012).

[34] A. A. Peshkov, D. Seipt, A. Surzhykov, and S. Fritzsche, Phys. Rev. A **96**, 023407 (2017).

[35] A. Afanasev, C. E. Carlson, C. T. Schmiegelow, J. Schulz, F. Schmidt-Kaler, and M. Solyanik, New J. Phys. **20**, 023032 (2018).

[36] B. Böning, W. Paufler, and S. Fritzsche, Phys. Rev. A **98**, 023407 (2018).

[37] A. Afanasev, C. E. Carlson, and H. Wang, J. Opt. **22**, 054001 (2020).

[38] J. D. Rodrigues, L. G. Marcassa, and J. T. Mendonça, J. Phys. B **49**, 074007 (2016).

[39] A. Surzhykov, D. Seipt, V. G. Serbo, and S. Fritzsche, Phys. Rev. A **91**, 013403 (2015).

[40] G. F. Quinteiro, F. Schmidt-Kaler, and C. T. Schmiegelow, Phys. Rev. Lett. **119**, 253203 (2017).

[41] H. M. Scholz-Marggraf, S. Fritzsche, V. G. Serbo, A. Afanasev, and A. Surzhykov, Phys. Rev. A **90**, 013425 (2014).

[42] V. P. Kosheleva, V. A. Zaytsev, R. A. Müller, A. Surzhykov, and S. Fritzsche, Phys. Rev. A **102**, 063115 (2020).

[43] A. A. Peshkov, V. G. Serbo, S. Fritzsche, and A. Surzhykov, Phys. Scr. **91**, 064001 (2016).

[44] A. Surzhykov, D. Seipt, and S. Fritzsche, Phys. Rev. A **94**, 033420 (2016).

[45] S. J. van Enk, Quantum Opt. **6**, 445 (1994).

[46] M. Babiker, C. R. Bennett, D. L. Andrews, and L. C. Dávila Romero, Phys. Rev. Lett. **89**, 143601 (2002).

[47] A. Alexandrescu, D. Cojoc, and E. Di Fabrizio, Phys. Rev. Lett. **96**, 243001 (2006).

[48] P. K. Mondal, B. Deb, and S. Majumder, Phys. Rev. A **89**, 063418 (2014).

[49] A. Afanasev, C. E. Carlson, and A. Mukherjee, J. Opt. Soc. Am. B **31**, 2721 (2014).

[50] R. Jáuregui, Phys. Rev. A **70**, 033415 (2004).

[51] A. R. Carter, M. Babiker, M. Al-Amri, and D. L. Andrews, Phys. Rev. A **72**, 043407 (2005).

[52] A. Afanasev, C. E. Carlson, and A. Mukherjee, Phys. Rev. Res. **3**, 023097 (2021).

[53] I. P. Ivanov, B. Liu, and P. Zhang, Phys. Rev. A **105**, 013522 (2022).

[54] M. Babiker, D. L. Andrews, and V. E. Lembessis, J. Opt. **21**, 013001 (2019).

[55] A. Muthukrishnan and C. R. Stroud, Jr., J. Opt. B **4**, S73 (2002).

[56] S. M. Barnett and M. V. Berry, J. Opt. **15**, 125701 (2013).

[57] H.-R. Chen, K.-Y. Lin, P.-K. Chen, N.-C. Chiu, J.-B. Wang, C.-A. Chen, P. Huang, S.-K. Yip, Y. Kawaguchi, and Y.-J. Lin, Phys. Rev. Lett. **121**, 113204 (2018).

[58] Y. Duan, Y. M. Bidasyuk, and A. Surzhykov, Phys. Rev. A **102**, 063328 (2020).

[59] F. Stopp, M. Verde, M. Katz, M. Drechsler, C. T. Schmiegelow, and F. Schmidt-Kaler, Phys. Rev. Lett. **129**, 263603 (2022).

[60] B. H. Bransden and C. J. Joachain, *Physics of Atoms and Molecules* (Prentice Hall, Harlow, England, 2003).

[61] D. J. Wineland, C. Monroe, W. M. Itano, D. Leibfried, B. E. King, and D. M. Meekhof, J. Res. Natl. Inst. Stand. Technol. **103**, 259 (1998).

[62] S. Flügge, *Practical Quantum Mechanics* (Springer-Verlag, Berlin, 1971).

[63] U. D. Jentschura and V. G. Serbo, Phys. Rev. Lett. **106**, 013001 (2011).

[64] O. Matula, A. G. Hayrapetyan, V. G. Serbo, A. Surzhykov, and S. Fritzsche, J. Phys. B **46**, 205002 (2013).

[65] J. Durnin, J. Opt. Soc. Am. A **4**, 651 (1987).

[66] J. Durnin, J. J. Miceli, Jr., and J. H. Eberly, Phys. Rev. Lett. **58**, 1499 (1987).

[67] M. E. Rose, *Elementary Theory of Angular Momentum* (Wiley & Sons, New York, 1957).

[68] N. N. Lebedev, *Special Functions and Their Applications* (Prentice-Hall, Englewood Cliffs, NJ, 1965).

[69] S. A. Akhmanov and S. Yu. Nikitin, *Physical Optics* (Clarendon, Oxford, 1997).

[70] M. Auzinsh, D. Budker, and S. M. Rochester, *Optically Polarized Atoms: Understanding Light-Atom Interactions* (Oxford University, Oxford, 2010).

[71] K. Blum, *Density Matrix Theory and Applications* (Springer, Berlin, 2012).

[72] L. von der Wense, P. V. Bilous, B. Seiferle, S. Stellmer, J. Weitenberg, P. G. Thirolf, A. Pálffy, and G. Kazakov, Eur. Phys. J. A **56**, 176 (2020).

[73] S. Stenholm, *Foundations of Laser Spectroscopy* (Wiley, New York, 1984).

[74] U. I. Safronova, M. S. Safronova, and W. R. Johnson, Phys. Rev. A **95**, 042507 (2017).

[75] R. V. Popov and A. V. Maiorova, Opt. Spectrosc. **122**, 366 (2017).

[76] V. G. Pal'chikov, Phys. Scr. **57**, 581 (1998).

[77] M. Abramowitz and I. A. Stegun, *Handbook of Mathematical Functions* (National Bureau of Standards, Washington, DC, 1964).